Available online at www.sciencedirect.com
ScienceDirect
Chemical Geology 245 (2007) 219–229
CHEMICAL GEOLOGY INCLUDING ISOTOPE GEOSCIENCE
www.elsevier.com/locate/chemgeo

Rate law for galena dissolution in acidic environment

Patricia Acero *, Jordi Cama [1], Carlos Ayora [1]

Institute of Earth Sciences "Jaume Almera", CSIC, c/ Lluís Solé i Sabarís s/n, Barcelona 08028, Spain

Received 14 May 2007; received in revised form 10 August 2007; accepted 13 August 2007

Editor: J. Fein

Abstract

A dissolution rate law for galena in acidic environment was derived from the steady-state dissolution rates using flow-through experiments. The influence of temperature, dissolved oxygen concentration and pH between 1 and 3 was assessed. This rate law can be used for predicting galena dissolution behavior in a wide range of conditions analogous to Acid Rock Drainage.

For pH below 2, the dissolution rate law can be expressed as:

$$R_{\mathrm{Gn,pH<2}} = 10^{-5.7\pm0.4} e^{\frac{-23\pm3}{RT}} a_{\mathrm{H^+}}^{0.43\pm0.05}$$

where R_{Gn} is the galena dissolution rate (mol m^{-2} s^{-1}), R is the gas constant (kJ mol^{-1} K^{-1}) , T is the temperature (K) and a_{H^+} is the activity of hydrogen ion in the solution.

Galena dissolution rate law for pH between 2 and 3 can be expressed as:

$$R_{\mathrm{Gn,pH=2-3}} = 10^{-8.5\pm0.4} e^{\frac{-15\pm2}{RT}} a_{\mathrm{H^+}}^{-0.78\pm0.04} a_{\mathrm{O_{2(aq)}}}^{0.30\pm0.03}$$

where $a_{O_{2(aq)}}$ is the activity of dissolved oxygen.

XPS (X-ray Photoelectron Spectroscopy) examination of the reacted galena samples shows the formation of a lead-deficient and sulfur-rich surface layer, consistent with the observed non-stoichiometry between dissolved sulfur and lead in all the studied solutions.

Based on the S/Pb ratio observed in solution and the reacted surfaces and the pH and dissolved oxygen dependence of the rates, two possible reactions for galena dissolution in acidic aqueous solution are proposed; (1) at pH ≤ 2 the rate seems to be determined by the protonation of surface sulfur atoms, and (2) at pH ≥ 2 the rate seems to be controlled by the attachment of oxygen to surface sulfur atoms.

The values obtained for the activation energies (15±2 kJ mol^{-1} at pH 3 and 23±3 kJ mol^{-1} at pH 1) suggest that galena dissolution is controlled by diffusion processes or mixed-controlled by diffusion of reactants and products between the bulk solutions and the reacting surfaces.

Keywords: Sulfides; Acid mine drainage; Dissolution kinetics; Lead

* Corresponding author. Present address: Petrology and Geochemistry Area, Earth Sciences Department, University of Zaragoza, Spain. Tel.: +34 976761000x3159; fax: +34 9761088.
E-mail address: patricia.acero@unizar.es (P. Acero).
[1] Tel.: +34 934095410; fax: +34 411 0012.

0009-2541/$ - see front matter © 2007 Elsevier B.V. All rights reserved.
doi:10.1016/j.chemgeo.2007.08.003

1. Introduction

Galena (PbS) is one of the most important sulfide minerals and the only lead mineral with economical interest. Together with other sulfide phases, galena is present in a large number of natural environments and mining sites and its weathering is very often an important source of pollution due to the release of lead to the soils, surface run-off and groundwaters. The mobility and potential toxicity associated to galena dissolution is increased in scenarios undergoing Acid Rock Drainage (ARD), not only because of the enhancement of the solubility of lead aqueous species at low pH but also because galena seems to dissolve faster in acidic aqueous solutions (Hsieh and Huang, 1989; De Giudici et al., 2005).

Owing to its environmental implications, many studies have focused on galena dissolution kinetics in the last years. Most of the earlier works have focused on the galena dissolution behavior in the very beginning of its interaction with solutions (a few hours to a few days) under different conditions of pH, dissolved oxygen and temperature. In one of the first kinetic studies, Hsieh and Huang (1989) studied the dissolution of galena at 20 °C and at pH from 2.5 to 9 and observed that galena dissolution rate was almost independent on the availability of dissolved oxygen but very pH-dependent, decreasing sharply when increasing pH in the studied range. Rimstidt et al. (1994) assessed the role of Fe(III) in galena dissolution at pH around 2 and pointed out that galena dissolution kinetics was substantially different from pyrite. More recently, De Giudici and Zuddas (2001) and De Giudici et al. (2005) studied the dissolution of freshly cleaved galena (001) surfaces at pH from 1 to around 6 and at temperatures ranging from 25 to 75 °C in short experiments (<150 h) and observed that galena dissolution rate increased with decreasing pH. Finally, two recent short batch studies (less than 1 h of interaction between galena and solutions) carried out under acidic conditions proposed that galena dissolution is non-oxidative (Pashkov et al., 2002; Zhang et al., 2004). Moreover, a first order dependence on $[H^+]$ was proposed by (Zhang et al., 2004) for the initial rate of galena dissolution within the pH range from 0.43 to 2.45 and in the presence of 1 mol l^{-1} NaCl solutions.

All these earlier studies have focused on the galena dissolution behavior in the very beginning of its interaction with solutions (a few hours to a few days). A short duration of experiments usually renders much faster dissolution rates than the ones obtained after months (or years) of interaction with solutions because there is no time for true steady state to be achieved. Hence, apparent rates obtained by short experiments are not applicable for predicting mineral dissolution in scenarios where an extended interaction with solutions is expected (e.g. in the pores of mine tailings or in acid streams). In line with this affirmation, galena dissolution rates obtained in earlier long-term dissolution experiments (Domènech et al., 2002; Cama et al., 2005) are up to three orders of magnitude slower than the initial rates.

Even though earlier studies have provided with a very valuable background on galena dissolution kinetics in the initial stages of interaction with solutions, the rates and reactions taking place during galena long-term dissolution remain almost unknown. In fact, within the acidic pH range, the steady-state dissolution rate has only been obtained at pH 3, at 25 °C and in solutions in equilibrium with atmospheric oxygen (Domènech et al., 2002; Cama et al., 2005).

In an attempt to bridge a part of the existing gap between data from short-term dissolution studies and field conditions, this paper is aimed at gaining insight into the galena long-term dissolution behavior. The main innovative aspect of this study with regard to previous works dealing with galena dissolution is that dissolution kinetic data were obtained at steady state. Therefore, the results obtained will be useful for predicting galena dissolution kinetics during extended interaction with acidic solutions, as in environments undergoing ARD. With this goal, the influence of temperature, hydrogen ion and dissolved oxygen concentrations at steady-state dissolution were exhaustively studied. As a result, a rate law accounting for the effects of these environmental factors on galena long-term dissolution was obtained. Moreover, the possible reactions controlling the overall galena dissolution within the range of the studied conditions were discussed, based on the observation of the evolution of solutions and reacting surfaces.

2. Materials and methods

2.1. Sample characterization

The galena sample used in this study was original from El Molar (Catalonian Coastal Range, Spain). X-ray Diffraction (XRD) was performed on thoroughly crushed samples using a Bruker D5005 difractometer with Cu Kα radiation. Powdered samples were scanned from 0 to 60° 2θ with a continuous scan at a rate of 0.083° 2θ per minute. XRD spectra of raw galena showed no evidence of the presence of any other mineral phase. Microprobe analysis was carried out in multiple points of the sample using an accelerating voltage of 20 kV and a beam current of 15 nA. The microprobe results confirmed the high

Table 1
Results (wt.% and at.%) of the microprobe analyses of galena used in the experiments

Element	Pb	S	Cu	Fe	Zn
wt.%	86.56	13.32	0.04	0.04	0.03
at.%	50.03	49.74	0.08	0.10	0.06

purity of the sample, which contained only trace amounts of copper, iron and zinc (Table 1).

Mineral samples were ground in agate mortar and sieved to obtain the fraction with particle sizes between 10 and 100 μm, used in the flow-through experiments. The specific surface area of the ground raw sample was determined to be $0.18 \pm 0.03\ m^2 \cdot g^{-1}$ by the BET method (Brunauer et al., 1938) using 5-point N_2 adsorption isotherms. Since the dissolution rates were to be normalized with respect to the surface area of the reacted samples, and provided that the powders resulting from usual milling operations do contain microparticles attached to the grains, no attempt of removing fine particles (smaller than 1 μm) adhered to the initial surfaces was done. On the other hand, one of the methodological advantages of flow-through experiments is that it is not necessary to carry out any pretreatment of the samples in order to eliminate the microparticles initially present. Since the dissolution rates are calculated once the steady state is attained and taking into account the specific surface corresponding to that stage, the effect of the sample grain size on the rate is completely corrected by normalization.

X-ray Photoelectron Spectroscopy (XPS) surface examination of the initial and reacted powdered samples, mounted on carbon conducive tabs, was carried out with a Physical Electronics (PHI) 5500 spectrometer using a monochromatic X-ray source (with an Al Kα line of 1486.6 eV energy and 350 W) placed perpendicular to the analyzer axis and calibrated using the 3d5/2 line of Ag with a width of 0.8 eV and a binding energy of 368.3 eV. All these measurements were made in an ultra high vacuum (UHV) chamber (pressure between $6.6 \cdot 10^{-11}$ and $6.6 \cdot 10^{-12}$ atm). The analyser pass energy was 23 eV. An electron flood gun at low energies (below 25 eV) was used for charge compensation. Comparison of the relative positions of the different peaks in all the studied spectra indicated that charge shifting can be considered uniform. In addition, examination of the peaks acquired simultaneously for carbon and oxygen did not show any asymmetry, which indicated that the asymmetry observed for lead peaks in the spectra were due to the presence of different species and not to charge compensation problems.

A deconvolution of the spectra into different components was carried out. Each spectrum was fitted by means of an iterative least-squares procedure with Gaussian–Lorentzian bands. Bulk-like spectra for the initial sample were obtained by using argon sputtering to remove any surface oxidation phase (Todd et al., 2003). Due to the low signal-to-noise ratio obtained for sulfur peaks in most of the spectra, they were only used as supplementary information for the deconvolution of lead peaks. Spectra are shown as raw data corrected for the peak shifting due to charge by adjusting the C1s peak (corresponding to adventitious carbon) to a binding energy of 284.6 eV.

Atomic concentrations of lead and sulfur in the mineral surfaces were determined from the XPS peak areas divided by atomic sensitivity factors, subsequent to Shirley background subtraction. According to the microprobe analysis, the initial sample was assumed to be perfectly stoichiometric. XPS analyses are shown as normalised to lead and sulfur. Loss of potentially present elemental sulfur could occur due to the lack of sample cooling while acquiring the measurements. Therefore, even if the presence of elemental sulfur was not confirmed, it will be considered as a possibility in the discussion below.

Finally, Scanning Electron Microscopy (SEM) was performed on selected Au and C-coated samples in order to observe the possible morphologic changes produced during dissolution. SEM examinations were carried out using an Hitachi H-4100FE instrument with intensity current between 15 and 20 kV.

2.2. Solutions

Input solutions of pH 1, 1.5, 2, 2.5 and 3 were prepared with analytical reagent grade hydrochloric (HCl) and sulfuric (H_2SO_4) acids and distilled, double deionized water (18.2 MΩ · cm). A Crison meter and combined glass electrode with temperature compensation was used to measure pH and was calibrated regularly with 2, 4 and 7 standard buffer solutions. Input and output pH was the same (within ±0.05 pH units). When possible, redox potential was measured by an Orion combination Pt/Ag–AgCl redox electrode. The measurements were corrected to be referenced to the Standard Hydrogen Electrode (SHE). Reliable redox potential measurements could not systematically be obtained because of a large drifting in the recorded values with time. This drifting can be caused by the low concentrations of aqueous species in the target solutions (in most cases less than 10^{-5} mol L^{-1}), by the presence of $H_2S(g)$ or even by the absence of a clearly dominant redox couple (Nordstrom, 2000). In the cases that the redox potential could be measured it was above 0.3 V.

Dissolved oxygen concentrations were determined using a Hanna portable meter with compensation of temperature, salinity and altitude with an accuracy of ±0.45 mg L^{-1}. Total lead and sulfur concentrations in the solutions were determined by Inductively Coupled Plasma Atomic Emission Spectrometry (ICP−AES) using a Thermo Jarrel-Ash instrument with CID detector. Calibration with sets of standards was performed and the regression coefficient exceeded 0.999. Three laboratory standards were analyzed with every 10 samples to check for accuracy and the error was estimated to be below 3%. The detection limits for Pb and S were determined to be $4.8 \cdot 10^{-8}$ and $3.5 \cdot 10^{-6}$mol L^{-1}, respectively.

2.3. Flow-through experiments

The experimental setup used in the present study has been described elsewhere (Cama and Acero, 2005). Experiments were carried out using stirred (Table 2, experiments GA1 to GA15) and non-stirred (NSGA16 to NSGA23) flow-through Lexan reactors with a reaction chamber of 40 mL in volume. Input solutions at the desired pH and DO concentrations were introduced in the reactors by means of a peristaltic pump with a flow rate between 0.027 and 0.050 mL min^{-1} (Table 2). Reactors were immersed in thermostatized water baths to keep the temperature at 25, 50 and 70 (±1) °C.

The experiments were carried out until steady state was reached. By convention, it was considered to be attained when differences in the metal concentration of the output solution were within ±10% for at least 200 h and four consecutive leachate samples.

To ensure the desired dissolved oxygen concentration, in the experiments carried out at dissolved oxygen conditions lower than those in equilibrium with a free atmosphere, input solutions were enclosed in a glove box purged with the corresponding O_2/N_2 gas mixtures (4.5% O_2 in N_2 for the experiment with 2.0 mg L^{-1} of dissolved oxygen and pure N_2 for the experiment with 0.2 mg L^{-1} of dissolved oxygen). Owing to the technical difficulties to keep the experiments stirred at the desired temperature into the glove box, the experiments GA10 to GA13 (Table 2) were carried out by fully immersing the stirred flow-through reactors and tubing into a thermostatized water

Table 2
Experimental conditions, steady-state values and obtained galena dissolution rates

Experiment	Acid type	Flow rate (mL min^{-1})	pH	DO (mg L^{-1})	T (°C)	Pb (mol L^{-1})	S (mol L^{-1})	S/Pb	Mass s.s (g)	Final BET area (m^2 g^{-1})	Rate Pb (mol m^{-2} s^{-1})	log (rate Pb)
GA1	HCl	0.042	3.0	8.7	25	$4.9 \cdot 10^{-5}$	$7.4 \cdot 10^{-6}$	0.1	0.76	0.30	$1.5 \cdot 10^{-10}$	−9.8
GA2	HCl	0.045	2.5	8.7	25	$1.6 \cdot 10^{-5}$	$7.0 \cdot 10^{-6}$	0.4	0.78	0.28	$5.7 \cdot 10^{-11}$	−10.2
GA3	HCl	0.040	2.0	8.7	25	$8.0 \cdot 10^{-6}$	b.d.l	–	0.78	0.33	$2.1 \cdot 10^{-11}$	−10.7
GA4	HCl	0.038	1.5	8.7	25	$1.9 \cdot 10^{-5}$	$1.1 \cdot 10^{-5}$	0.6	0.75	0.36	$4.3 \cdot 10^{-11}$	−10.4
GA5	HCl	0.042	1.0	8.7	25	$2.1 \cdot 10^{-5}$	b.d.l	–	0.80	0.28	$6.4 \cdot 10^{-11}$	−10.2
GA6	HCl	0.041	3.0	8.7	50	$6.4 \cdot 10^{-5}$	b.d.l	–	0.76	0.27	$2.2 \cdot 10^{-10}$	−9.7
GA7	HCl	0.027	1.0	8.7	50	$6.2 \cdot 10^{-5}$	b.d.l	–	0.78	0.32	$1.1 \cdot 10^{-10}$	−9.9
GA8	HCl	0.039	3.0	8.7	70	$1.0 \cdot 10^{-4}$	$7.0 \cdot 10^{-6}$	0.1	0.73	0.28	$3.3 \cdot 10^{-10}$	−9.5
GA9	HCl	0.027	1.0	8.7	70	$9.6 \cdot 10^{-5}$	$9.2 \cdot 10^{-6}$	0.1	0.77	0.25	$2.2 \cdot 10^{-10}$	−9.7
GA10	HCl	0.033	3.0	2.0	25	$3.4 \cdot 10^{-5}$	$5.0 \cdot 10^{-6}$	0.1	0.77	0.30	$8.0 \cdot 10^{-11}$	−10.1
GA11	HCl	0.034	3.0	0.2	25	$1.9 \cdot 10^{-5}$	$6.5 \cdot 10^{-6}$	0.1	0.76	0.32	$4.6 \cdot 10^{-11}$	−10.3
GA12	HCl	0.033	1.0	2.0	25	$2.0 \cdot 10^{-5}$	b.d.l	–	0.76	0.27	$5.5 \cdot 10^{-11}$	−10.3
GA13	HCl	0.033	1.0	0.2	25	$2.3 \cdot 10^{-5}$	b.d.l	–	0.77	0.35	$4.6 \cdot 10^{-11}$	−10.3
GA14	H_2SO_4	0.045	1.0	8.7	25	$1.5 \cdot 10^{-5}$	n.d.	–	0.80	0.26	$5.3 \cdot 10^{-11}$	−10.3
GA15	H_2SO_4	0.028	3.0	8.7	25	$6.0 \cdot 10^{-5}$	n.d.	–	0.78	0.31	$1.1 \cdot 10^{-10}$	−9.9
NSGA16	HCl	0.029	3.0	8.7	25	$2.3 \cdot 10^{-5}$	$6.6 \cdot 10^{-6}$	0.3	0.22	0.30	$1.6 \cdot 10^{-10}$	−9.8
NSGA17	HCl	0.027	2.0	8.7	25	$7.0 \cdot 10^{-6}$	b.d.l	–	0.42	0.30	$2.5 \cdot 10^{-11}$	−10.6
NSGA18	HCl	0.027	1.0	8.7	25	$1.8 \cdot 10^{-5}$	b.d.l	–	0.42	0.30	$7.0 \cdot 10^{-11}$	−10.2
NSGA19	HCl	0.045	3.0	0.2	25	$1.3 \cdot 10^{-5}$	b.d.l	–	0.79	0.27	$4.7 \cdot 10^{-11}$	−10.3
NSGA20	HCl	0.034	1.0	0.2	25	$1.2 \cdot 10^{-5}$	b.d.l	–	0.75	0.24	$3.7 \cdot 10^{-11}$	−10.4
NSGA21	HCl	0.049	3.0	8.7	50	$1.9 \cdot 10^{-5}$	b.d.l	–	0.22	0.30	$2.4 \cdot 10^{-10}$	−9.6
NSGA22	HCl	0.049	3.0	8.7	70	$2.2 \cdot 10^{-5}$	b.d.l	–	0.21	0.30	$2.8 \cdot 10^{-10}$	−9.5
NSGA23	HCl	0.050	1.0	8.7	50	$4.9 \cdot 10^{-5}$	$4.1 \cdot 10^{-6}$	0.1	0.77	0.36	$1.5 \cdot 10^{-10}$	−9.8

Experiments GA1 through GA15 were stirred and experiments NSGA16 through NSGA23 were non-stirred.
s.s. = steady state.
b.d.l. = below detection limit for S ($3.5 \cdot 10^{-6}$ mol L^{-1}).
n.d. = not determined (dissolved sulfur in experiments carried out with sulfuric acid).
The initial surface area in all the experiments was 0.18 m^2 g^{-1}. S/Pb represents the ratio between measured sulfur and lead concentrations in solution.

bath attached to the glove box in order to prevent any atmospheric oxygen diffusion into the system. The validity of the obtained rates was examined by carrying out two additional non-stirred experiments (Table 2, experiments NSGA19 and NSGA20) under virtually anoxic conditions analogous to experiments GA11 and GA13 (0.2 mg L^{-1} of dissolved oxygen), but enclosing the whole experimental set-up (input and output solutions, pumps and tubing) into the glove box. In both types of experimental set-up, input solutions were also purged with the same gas mixtures filling the glove box on a regular basis to ensure the desired dissolved oxygen concentrations, which were checked before pumping into the reactors. The dissolution rates obtained in the respective duplicates were the same, within error, proving the validity of results (Table 2). Dissolved oxygen variations in the output solutions were not continuously monitored because they were found to be within measurement error during previous experimental tests.

After the experiments, the reacted samples were collected, rinsed with double-distilled water, dried at room temperature and stored in closed microvials until examination by Scanning Electron Microscopy (SEM), X-Ray Photoelectron Spectroscopy (XPS) and determination of their BET surface area.

2.4. Calculation of steady-state dissolution rates

In a flow-through reactor, the steady-state dissolution rate (r, in mol·m^{-2}· s^{-1}) is calculated according to the following simple mass-balance equation

$$r = \frac{q(c_i - c_i^0)}{v_i A} \quad (1)$$

where q is the flow rate of the solution through the reactor, v_i is the stoichiometric coefficient of the i element in the studied material and A is the total surface area of the mineral sample, in area units. The notations c_i and c_i^0 represent the out and in-flowing concentrations of the i element, respectively.

The error associated with the calculated dissolution rates was calculated by the Gaussian error propagation method (Barrante, 1974) to be around 16% and it was dominated by the uncertainty of BET surface area measurements (±15%).

3. Results and discussion

The steady-state results of the flow-through experiments are presented in Table 2. Most of the experiments ran for 1200 to 1800 h, attaining steady state only after 500 to 1000 h of interaction with the solutions. Steady state was maintained in most cases for more than 300 h and calculated total dissolved mass of galena throughout the experiments was in all cases less than 5% of the initial mass of the sample.

Lead and sulfur concentrations in the output solutions were highest at the start of the experiments, decreasing thereafter until steady state was attained (Fig. 1). Sulfur concentrations in the output solutions were always lower than the lead concentrations and $H_2S_{(g)}$ odour was noticed during collection of some of the output solutions. Hence, dissolution rates were based only on lead concentrations. Sulfur deficit in solution has not only been described in earlier works on galena dissolution (Fornasiero et al., 1994a; De Giudici and Zuddas, 2001; Pashkov et al. 2002; Cama and Acero, 2005; Cama et al., 2005; De Giudici et al., 2005) but also in studies on the dissolution of other sulfide minerals, such as pyrite (Domènech et al., 2002); pyrrhotite (Janzen et al., 2000), chalcopyrite (Lu et al., 2000; Devi et al., 2000; Antonijevic and Bogdanovic, 2004) or sphalerite (Buckley et al., 1989; Lochmann and Pedlik, 1995; Weisener et al., 2003, 2004).

Dissolution rates were normalized to the estimated final mass and BET surface area. The solution saturation state was estimated assuming congruent galena dissolution. According to calculations run with the PHREEQC code (Parkhurst, 1995) using the lowest measured redox potential, output solutions were unsaturated with respect to galena or anglesite ($PbSO_4$). The only exceptions were the experiments carried out using sulfuric acid solution (experiments GA14 and GA15) in which supersaturation with respect to anglesite was observed. However,

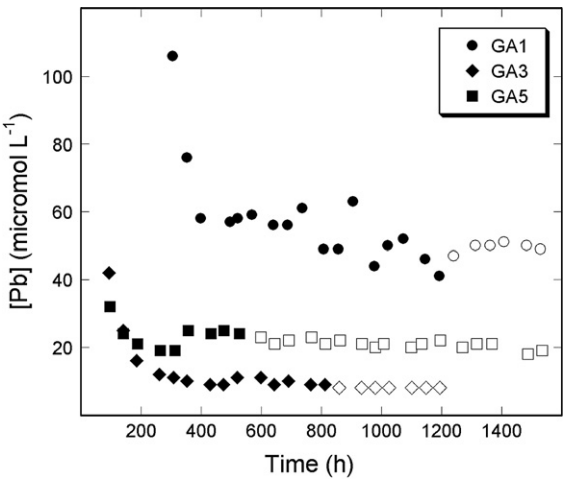

Fig. 1. Variation in lead concentrations as a function of time in three representative experiments at pH 3 (experiment GA1), pH 2 (GA3) and 1 (GA5). Open symbols denote values of lead concentrations used to calculate average steady states. Initial concentrations at pH 3 are omitted to improve the quality of the figure.

anglesite precipitation was unlikely in any of those experiments since XPS results did not show the presence of lead sulfate in any of those samples.

Galena dissolution rates obtained in the experiments carried out using sulfuric acid were the same (within error) as the rates obtained under the same experimental conditions using hydrochloric acid. Likewise, the dissolution rates obtained in the non-stirred experiments (NSGA16 to NSGA23) showed a good agreement with the rates obtained using stirred reactors under analogous experimental conditions (Table 2). This coincidence between the rates obtained with different leachants and types of reactors proves the good reproducibility of results.

A comparison of SEM images of samples before and after the experiments (Fig. 2) showed that a fraction of the initial microparticles attached to the galena surfaces disappeared over the experiments. Some dissolution features, such as terrace retreat and etch-pitch formation, can also be observed in the reacted samples. The presence of sulfate or elemental sulfur precipitates over the reacted surface was not observed.

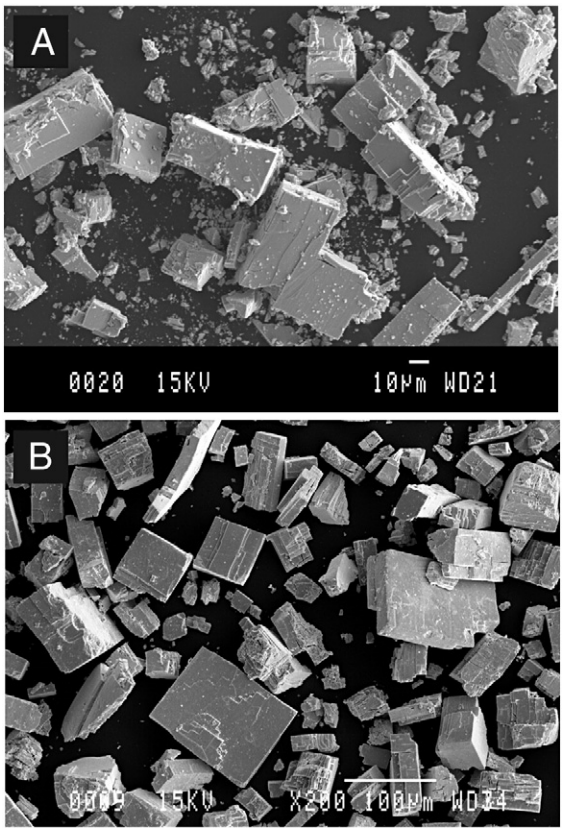

Fig. 2. SEM images of the samples used in the experiments. (A) Freshly ground and sieved galena before the experiments, and (B) galena grains after dissolution experiment.

Table 3
Results obtained by the X-ray Photoelectron Spectroscopy (XPS) determinations on the initial and reacted samples

Sample	Pb	S	S/Pb	Pbs	Pb–O/Pb–OH/Pb–S_2O_3/Pb–SO_3	$PbSO_4$
				137–137.8 eV	138.3–138.9 eV	139.2 eV
	at.%[a]			% over total Pb species		
Initial PbS	50	50	1.0	38	62	–
GA1	31	69	2.3	46	54	–
GA2	27	73	2.6	58	42	–
GA3	30	70	2.3	–	87	13
GA4	31	69	2.2	53	47	–
GA5	33	67	2.0	43	57	–
GA6	30	70	2.3	33	67	–
GA7	35	65	1.8	100	–	–
GA8	33	67	2.0	73	27	–
GA9	39	61	1.5	72	28	–
GA10	34	66	1.9	59	41	–
GA11	30	70	2.4	100	–	–
GA12	31	69	2.2	69	31	–
GA13	26	74	2.9	44	56	–
GA14	36	64	1.8	74	26	–
GA15	34	66	2.0	80	20	–

S/Pb represents the ratio between the atomic concentrations of sulfur and lead in the initial and reacted galena surfaces, as estimated by XPS.
[a]Normalising out the rest of elements (oxygen and adventicious carbon).

The results obtained by XPS examination of the samples before and after the flow-through experiments are presented in Table 3. The surface S/Pb ratios showed a marked S enrichment and Pb deficiency in all the reacted samples when compared with the initial unreacted surface, in agreement with many earlier works (Sun et al., 1991; Kim et al., 1996; Mikhlin et al., 2006 and references therein). The Pb4f region (Fig. 3) contains the contribution of Pb4f5/2 and Pb4f7/2 that are due to spin-orbit splitting. According to this splitting, an area ratio for Pb4f5/2 to Pb4f7/2 of 0.75 and a position shifting of 4.86 eV was fixed during deconvolution of lead peaks. The Pf4f7/2 peak maxima were generally found at binding energies between 137.0–137.8 eV, which was considered to correspond to the bulk lead sulfide (Fornasiero et al., 1994b and references therein; De Giudici et al., 2005). Another minor contribution to the Pf4f7/2 peak was found at binding energies between 138.3–138.9 eV. This range of energies could correspond to lead (oxy)hydroxide (Nowak et al., 2000; De Giudici et al., 2005), sulfite (Zinng and Hercules, 1978) or thiosulfate (Fornasiero et al., 1994b). Although that range of energies was attributed to lead chloride in some earlier works (Pederson, 1982; De Giudici et al., 2005), it is worth noting the clear presence of a species at those

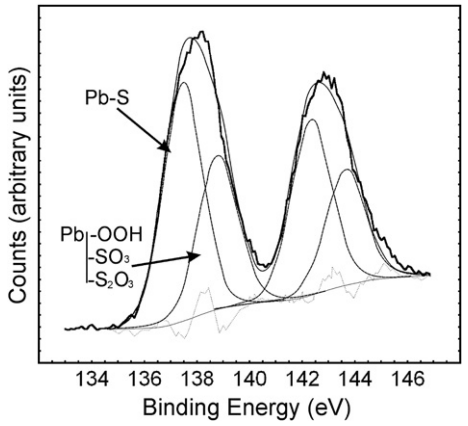

Fig. 3. Curve fitted Pb4f spectra of representative sample after the flow-through experiments. The position of the fitted species has been detailed in the text.

energies in our experiments carried out in sulfuric instead of hydrochloric acid.

S2p peak results were consistent with lead peaks deconvolution. Sulfate species were present only in the GA3 sample and two other sulfur species could be identified in most of the samples at binding energies of 160.4–161.2 eV and 162–163 eV, respectively. The former can be attributed to surface sulfide (Fornasiero et al., 1994b and references therein; Smart et al., 1999 and references therein; De Giudici et al., 2005). For the latter, energies in the 162–163 eV range have been previously considered to correspond to lead di- or polysulfides (Smart et al., 1999 and references therein). However, taking into account the low signal-to-noise ratio obtained in our S2p peaks and the lack of references justifying the assignment of any of the detected lead species to lead polysulfides, this interpretation would be somewhat arbitrary. As explained above, the presence of elemental sulfur on the surfaces could not be confirmed by XPS. However, evidence of the formation of islands of elemental sulfur in acid solution has been provided in earlier XPS and AFM works (Kartio et al., 1998; De Giudici and Zuddas, 2001; Cama et al., 2005).

4. Discussion

4.1. Significance of steady-state dissolution rates of galena

The observed galena dissolution rates are generally between two and three orders of magnitude slower than those obtained in earlier short studies (Table 4). This difference may be attributed in part to the fact that, in those studies, rates were generally normalized to initial and not to final specific areas. However, the main cause of the difference must be the shorter duration (less than 150 h) of the experiments in those works compared with the longer experimental runs in our flow-through experiments. It is very common that concentrations are highest at the beginning of the dissolution experiments, decreasing thereafter until steady state is attained. Such evolution has been previously reported not only for galena (De Giudici and Zuddas, 2001; Cama et al., 2005; De Giudici et al., 2005) but also for other sulfides, such as pyrite (Domènech et al., 2002), chalcopyrite (Acero et al., 2007) or sphalerite (Weisener et al., 2003) and even for other types of minerals (Metz and Ganor, 2001; Brandt et al., 2003). High concentrations at the beginning of the experiments are due to either dissolution of an outer layer of the reacting mineral, which may be altered by grinding or cleaving, or to dissolution of microparticles with higher specific surface areas than the bulk sample (Lasaga, 1998).

Table 4
Methodology, dissolution rates and apparent activation energies obtained in earlier studies on galena dissolution kinetics and in the present work

Reference	Experiment type	Duration (h)	Rate (mol m^{-2} s^{-1})	pH	O_2^a	T (°C)	E_{app}^b (kJ mol^{-1})
De Giudici and Zuddas (2001)	Flow through HCl (fragment)	44	$4.5 \cdot 10^{-8}$	1	21	20	–
Domènech et al. (2002)	Flow through HCl (powder)	>800	$2.8 \cdot 10^{-10}$	3.05	21	25	–
Zhang et al. (2004)	Batch HCl+1 M NaCl	<1	$4.4 \cdot 10^{-8}$	0.93	–	25	43.54
De Giudici et al. (2005)	Flow through HCl (fragment)	<150	$3.74 \cdot 10^{-7}$	1.2	21	25	13.5±2
		<150	$1.59 \cdot 10^{-7}$	2.87	21	25	13.5±2
Cama et al. (2005)	Flow through HCl and HNO_3 (fragment)	1	$5.1 \cdot 10^{-7}$	3	21	20	–
		<200	$6.8 \cdot 10^{-7}$	2	21	20	–
		3	$3.4 \cdot 10^{-6}$	1	21	20	–
	Flow through HCl (powder)	>1500	$1.3 \cdot 10^{-10}$	3	21	25	–
This study	Flow through HCl and H_2SO_4 (powder)	1200–1800	$6.2 \cdot 10^{-11}$	1	21	25	23±3
		1200–1800	$2.3 \cdot 10^{-11}$	2	21	25	–
		1200–1800	$1.4 \cdot 10^{-10}$	3	21	25	15±2

[a] In partial pressure in equilibrium with the solution.
[b] Apparent Activation Energy in similar temperature range for comparison.

As explained above, steady state in flow-through experiments was attained only after 500 to 1000 h of interaction with the solutions. If lead concentrations at the beginning of our experiments were considered to be in steady state, rates much closer to those previously reported would have been obtained. In line with this explanation, the galena dissolution rates obtained in the present study match very closely the rates proposed by Domènech et al. (2002) and Cama et al. (2005), which carried out the only earlier long-term dissolution studies (Table 4).

This discrepancy between initial and long-term dissolution rates highlights the necessity of finding dissolution rates based on true steady state if prediction of the long term behavior is intended. Even though batch or mixed flow-through experiments can be very useful to gain insight into the reactions and mechanisms involved in heterogeneous reactions, their results can not be applied a priori for quantitative, long term prediction.

As described in Section 3, the dissolution rates obtained in the experiments carried out in sulfuric acid were the same, within error, as the rates obtained in hydrochloric acid. Therefore, the type of electrolyte used does not seem to exert any influence on galena dissolution under the studied conditions. Hence, the dissolution rates here presented can be used in prediction of galena dissolution behavior in natural ARD, in which sulfate is the main anionic species.

4.2. Effects of pH, DO and temperature on galena dissolution rates

The variation of the galena dissolution rate with pH at 25 °C and 8.7 mg L^{-1} DO is shown in Fig. 4.Two different trends in the dissolution rate with pH variations

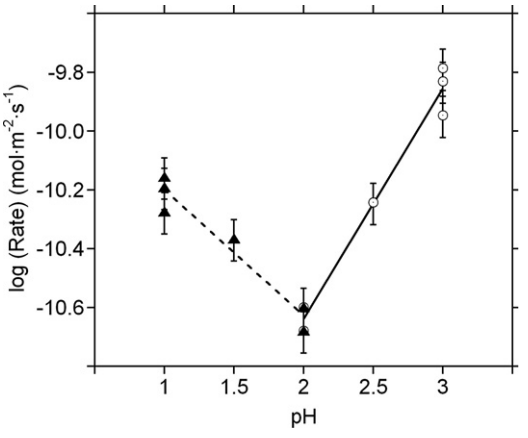

Fig. 4. Galena dissolution rate dependence on pH at 25 °C and 8.7 mg L^{-1} of dissolved oxygen.

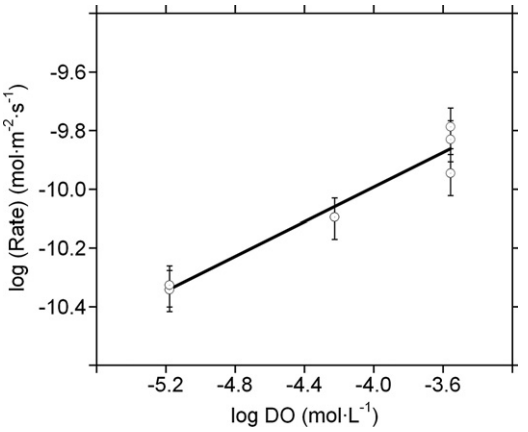

Fig. 5. Galena dissolution rate dependence on dissolved oxygen at pH 3 and 25 °C.

can be clearly appreciated. Whereas for pH values between 2 and 3, the rates increased with pH increase, a decrease in pH below 2 increased the galena dissolution rate. Consequently, the minimum rate was obtained at pH 2. This evolution of the rates with pH was clearly observed in replicate experiments (Table 2 and Fig. 4).

Calculation of the reaction order of galena dissolution with respect to a_{H^+} yielded a value of 0.43 ± 0.05 for pH values below 2 and -0.78 ± 0.04 for pH values above 2. The reaction order with respect to the hydrogen ion activity at pH below 2 is lower than the order 1 previously proposed by Zhang et al. (2004), which can only be attributed to differences in the type of experiment carried out (long-term flow-through vs. short batch experiments).

The dependence of galena dissolution rate on dissolved oxygen concentration and temperature was assessed at two different pH values (pH 1 and 3), representing the two pH ranges with different pH-dependence of the rate. Rates obtained at 25 °C and at three different dissolved oxygen concentrations (8.7, 2.1 and 0.2 mg L^{-1}) showed that the galena dissolution rate at pH 3 is DO-dependent, decreasing when the dissolved oxygen concentration decreases (Fig. 5). This type of dependence has been previously reported for other sulfide minerals, such as pyrite (Nicholson et al., 1988; Williamson and Rimstidt, 1994; Domènech et al., 2002). Reaction order of galena dissolution rate with respect to dissolved oxygen at pH 3 was calculated to be 0.30 ± 0.03.

On the contrary, galena dissolution rate is independent of dissolved oxygen concentrations at pH 1, being the rates obtained at the three different dissolved oxygen concentrations the same within error (Table 2). This variation on the DO-dependence of the dissolution rates

with pH suggests that different dissolution reactions are predominant at different pH ranges.

To obtain the apparent activation energies, several experiments were carried out at 25, 50 and 70 (±1 °C) whilst maintaining both pH and dissolved oxygen concentration constant (pH 1 or 3 and 8.7 mg L^{-1} of dissolved oxygen). The dissolution rates obtained are shown in Table 2 and in Fig. 6. The value obtained for the apparent activation energy was 23±3 kJ mol^{-1} at pH 1 and 15±2 at pH 3.

4.3. Galena dissolution rate law

Overall dissolution rate of a mineral within a certain range of far-from-equilibrium conditions is proportional to a fractional power of the activity of catalysts or inhibitors, according to (modified from Lasaga et al., 1994):

$$r = k\, e^{-E_a/\mathrm{RT}} \prod_i a_i^{n_i} \quad (2)$$

where k is a rate constant, E_a is the apparent activation energy of the overall dissolution reaction, R is the gas constant, T is the temperature (K). In Eq. (2), a_i represents the activity of any other species in solution which could have catalytic or inhibitory effect in the overall dissolution rate, being n_i the reaction order of the dissolution rate with respect to a_i.

The deduced reaction orders of the galena dissolution rate with respect to the H^+ activity, the dissolved oxygen activity, the apparent activation energy (E_a) and the dissolution constant (k), estimated from multiple linear regression of the experimental dissolution rates, yield the galena dissolution rate laws. For pH below 2, the galena dissolution rate law can be expressed as:

$$R_{\mathrm{Gn,pH<2}} = 10^{-5.7\pm0.4} e^{\frac{-23\pm3}{\mathrm{RT}}} a_{\mathrm{H^+}}^{0.43\pm0.05} \quad (3)$$

where R_{Gn} is the galena dissolution rate (mol m^{-2} s^{-1}), R is the gas constant (kJ mol^{-1} K^{-1}) , T is the temperature (K) and a_{H^+} is the activity of H^+ in solution.

At pH between 2 and 3, the rate law for galena dissolution can be expressed as

$$R_{\mathrm{Gn,pH=2-3}} = 10^{-8.5\pm0.4} e^{\frac{-15\pm2}{\mathrm{RT}}} a_{\mathrm{H^+}}^{-0.78\pm0.04} a_{\mathrm{O_{2(aq)}}}^{0.30\pm0.03} \quad (4)$$

where $a_{\mathrm{O_{2(aq)}}}$ is the activity of dissolved oxygen.

4.4. Galena dissolution reactions

Galena dissolution rates exhibited a clear pH-dependence within the range of conditions studied in this paper, being lowest at pH around 2 and increasing from that point with any increase or decrease in the hydrogen ion activity in solution.

In the pH range from 1 to 2 dissolution rates were independent of the dissolved oxygen concentrations but increased when H^+ activity in solution was increased. This behavior is consistent with a dissolution reaction consisting in protonation of the galena surface. The only protonation mechanism that has been proven to be energetically favorable in aqueous solution consists of attachment of three H^+ onto three surface S atoms surrounding a central Pb atom, which is then replaced by a fourth H^+ (Gerson and O'Dea, 2003). According to these authors, the subsequent removal of $H_2S_{(aq)}$ following a second protonation of any of the surface S atoms is energetically unfavorable, which could lead to the formation of a Pb-deficient S-rich surface as observed in this study and in earlier works (Sun et al., 1991; Kim et al., 1996; Mikhlin et al., 2006 and references therein). Although the non-stoichiometry S/Pb in solution and the XPS examination of the reacted surfaces in our experiments are both perfectly consistent with that hypothesis, the observed $H_2S_{(g)}$ volatilization suggests that a fraction of surface sulfur is released to solution as HS^-, forming thereafter $H_2S_{(aq)}$, which can be transformed to $H_2S_{(g)}$ and lost.

In the range of pH from 2 to 3, galena dissolution rates increased with decreasing pH and also with increasing dissolved oxygen concentrations. These differences in behavior, compared to the range from 1 to 2, suggest that different rate-determining reactions were taking place. The fact that galena dissolution rates depend on the dissolved oxygen concentration suggests that the rate-controlling dissolution reaction within this pH range is oxidative. The results obtained in our experiments are consistent with, at

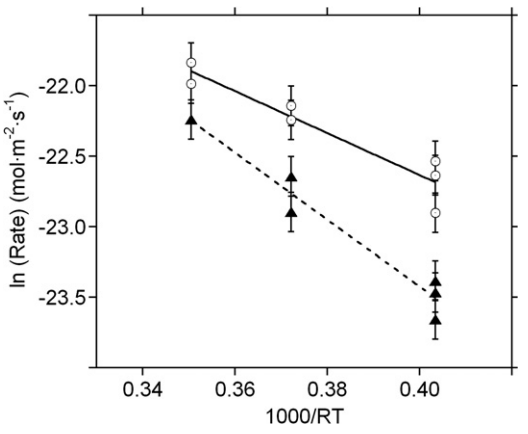

Fig. 6. Galena dissolution rate dependence on temperature at pH 1 (triangles) and 3 (circles) and 8.7 mg L^{-1} of dissolved oxygen.

least, one of the mechanisms for acidic aerobic dissolution proposed by Gerson and O'Dea (2003). According to these authors, an energetically possible mechanism of galena oxidative dissolution is initiated when molecular O_2 spontaneously disassociates if placed diagonally between two surface S atoms. However, in acidic aqueous solutions, a fraction of sulfur surface atoms must be protonated. It seems clear that the more protonated the galena surface, the more difficult the attachment of oxygen to sulfur surface atoms. This hypothesis would explain why galena dissolution rates decreased with pH decreasing from 3 to 2. In line with this hypothesis, the fact that the minimum rates were obtained at pH 2 would be related to the presence around that pH value of the point of zero net charge (PZNC) for galena. Although previously reported $PZNC_{galena}$ are fairly disperse, there is an almost general agreement for values between 1.4 and 3 (Hsieh and Huang, 1989 and references therein; Bebie et al., 1998).

The obtained apparent activation energies were around 20 kJ mol^{-1} (23 kJ mol^{-1} at pH 1 and 15 kJ mol^{-1} at pH 3). Values of the activation energy lower than 20 kJ mol^{-1} are usually considered to be associated with diffusion-controlled dissolution kinetics, whereas higher values are usually attributed to surface reaction control (Lasaga, 1998), at least in silicates. According to these observations, galena dissolution seems to be controlled by diffusion processes or mixed-controlled by diffusion and surface processes. When the dissolution of a mineral is diffusion-controlled, the dissolution rate is expected to vary if the stirring rate is changed (Berner, 1980). As explained in Section 3, dissolution rates obtained with and without stirring were always the same within error under the experimental conditions presented in this paper. At present, we do not have any explanation for this apparent contradiction between diffusion-control and lack of variation of the rates with stirring, but future research on this topic is granted.

5. Conclusions

Galena dissolution rates and reactions were studied by means of stirred and non-stirred flow-through experiments at pH from 1 to 3, at temperatures from 25 to 70 °C and under three different dissolved oxygen concentrations. The obtained results showed that galena dissolution rate is lowest at pH around 2, increasing from that point with any increase or decrease in the pH. The reaction order with respect to H^+ activity was found to be 0.43 ± 0.05 at pH below 2 and -0.78 ± 0.04 from pH 2 to 3.

At pH 1, galena dissolution rates were independent of the dissolved oxygen concentrations, whereas at pH 3 dissolution rates increased with increasing dissolved oxygen activity. In this last case, the reaction order with respect to the dissolved oxygen activity was found to be 0.30 ± 0.03.

Measured dissolution rates increased with temperature, yielding apparent activation energies of 23 ± 3 kJ mol^{-1} at pH 1 and 15 ± 2 kJ mol^{-1} at pH 3. Both energy values are consistent with a kinetic regime controlled by diffusion processes or mixed-controlled by diffusion and surface reactions.

XPS examination of the samples showed that galena reacted surfaces were metal-deficient and S-rich compared to the initial unreacted sample. Taking into account the variations of the galena dissolution rate with pH and dissolved oxygen, the low S/Pb ratio in solution for all the experiments carried out, the XPS results and previously published thermodynamic calculations by Gerson and O'Dea (2003), two possible galena dissolution reactions are proposed; 1) protonation of surface S atoms with subsequent formation of a sulfur-rich surface layer and release of a part of sulfur as HS^-, and 2) disassociation of molecular O_2 and attachment to two surface sulfur atoms, with subsequent release of lead and sulfur.

Acknowledgements

This work was funded by the Research and Development Contracts REN 2000-1003-C03-01 and REN 2003-0950-C04-02 with the Spanish Government. PA was financially supported by the Spanish Government with PhD fellowship. We gratefully acknowledge the fruitful discussions with Araceli Garrido and Volker Metz and the analytical assistance of Javier Pérez, Rafael Bartrolí, Mercè Cabanes, Silvia Martínez and Josep Elvira from the Instituto de Ciencias de la Tierra "Jaume Almera"-CSIC, and Lorenzo Calvo, Joaquim Portillo and Joan Gámez from the SCT of the University of Barcelona. We thank the Editor, Dr Jeremy B. Fein, for his help and comments. The constructive criticisms from Dr. J.D. Rimstidt and an anonymous reviewer have significantly improved the original manuscript.

References

Acero, P., Cama, J., Ayora, C., 2007. Kinetics of chalcopyrite dissolution at pH 3. Eur. J. Mineral. 19 (2), 173–182.

Antonijevic, M., Bogdanovic, G., 2004. Investigation of the leaching of chalcopyritic ore in acidic solutions. Hydrometallurgy 73 (3–4), 245–256.

Barrante, J., 1974. Applied Mathematics for Physical Chemistry. Prentice-Hall, Inc.

Bebie, J., Schoonen, M., Fuhrmann, M., Strongin, D., 1998. Surface charge development on transition metal sulfides: an electrokinetic study. Geochim. Cosmochim. Acta 62 (4), 633–642.

Berner, R.A., 1980. Early diagenesis; a theoretical approach. Princeton Series in Geochemistry. Princeton University Press.

Brandt, F., Bosbach, D., Krawczyk-Barsch, E., Arnold, T., Bernhard, G., 2003. Chlorite dissolution in the acid pH-range: a combined microscopic and macroscopic approach. Geochim. Cosmochim. Acta 67 (8), 1451–1461.

Brunauer, S., Emmet, P., Teller, E., 1938. Adsorption of gases in multimolecular layers. J. Am. Chem. Soc. 60, 309–319.

Buckley, A., Woods, R., Wouterlood, H., 1989. An XPS investigation of the surface of natural sphalerites under flotation-related conditions. Int. J. Miner. Process. 26 (1–2), 29–49.

Cama, J., Acero, P., 2005. Dissolution of minor sulphides present in a pyritic sludge at pH 3 and 25 °C. Geol. Acta 3, 15–26.

Cama, J., Acero, P., Ayora, C., Lobo, A., 2005. Galena surface reactivity at acidic pH and 25 °C based on flow-through and in situ AFM experiments. Chem. Geol. 214 (3–4), 309–330.

De Giudici, G., Zuddas, P., 2001. In situ investigation of galena dissolution in oxygen saturated solution: evolution of surface features and kinetic rate. Geochim. Cosmochim. Acta 65 (9), 1381–1389.

De Giudici, G., Rossi, A., Fanfani, L., Lattanzi, P., 2005. Mechanisms of galena dissolution in oxygen-saturated solutions: evaluation of pH effect on apparent activation energies and mineral-water interface. Geochim. Cosmochim. Acta 69 (9), 2321–2331.

Devi, N., Madhuchhanda, M., Rao, K., Rath, P., Paramguru, R., 2000. Oxidation of chalcopyrite in the presence of manganese dioxide in hydrochloric acid medium. Hydrometallurgy 57 (1), 57–76.

Domènech, C., de Pablo, J., Ayora, C., 2002. Oxidative dissolution of pyritic sludge from the Aznalcollar mine (SW Spain). Chem. Geol. 190 (1–4), 339–353.

Fornasiero, D., Li, F., Ralston, J., 1994a. Oxidation of Galena II. Electrokinetic Study. J. Colloid Interface Sci. 164 (2), 345–354.

Fornasiero, D., Li, F., Ralston, J., Smart, R.S.C., 1994b. Oxidation of Galena surfaces I. X-ray photoelectron spectroscopic and dissolution kinetic studies. J. Colloid Interface Sci. 164 (2), 333–344.

Gerson, A., O'Dea, A., 2003. A quantum chemical investigation of the oxidation and dissolution mechanisms of Galena. Geochim. Cosmochim. Acta 67 (5), 813–822.

Hsieh, Y., Huang, C., 1989. The dissolution of PbS(s) in dilute aqueous solutions. J. Colloid Interface Sci. 131 (2), 537–549.

Janzen, M., Nicholson, R., Scharer, J., 2000. Pyrrhotite reaction kinetics: reaction rates for oxidation by oxygen, ferric iron, and for nonoxidative dissolution. Geochim. Cosmochim. Acta 64 (9), 1511–1522.

Kartio, I., Laajalehto, K., Suoninen, E., Buckley, A., Woods, R., 1998. The initial products of the anodic oxidation of galena in acidic solution and the influence of mineral stoichiometry. Colloids Surf., A Physicochem. Eng. Asp. 133 (3), 303–311.

Kim, B.S., Hayes, R., Prestidge, C., Ralston, J., Smart, R.S.C., 1996. In-situ scanning tunnelling microscopy studies of galena surfaces under flotation-related conditions. Colloids Surf., A Physicochem. Eng. Asp. 117 (1–2), 117–129.

Lasaga, A., 1998. Kinetic Theory in the Earth Sciences. Princeton Series in Geochemistry. Princeton University Press, Princeton, New Jersey.

Lasaga, A., Soler, J., Ganor, J., Burch, T., Nagy, K., 1994. Chemical weathering rate laws and global geochemical cycles. Geochim. Cosmochim. Acta 58 (10), 2361–2386.

Lochmann, J., Pedlik, M., 1995. Kinetic anomalies of dissolution of sphalerite in ferric sulfate solution. Hydrometallurgy 37 (1), 89–96.

Lu, Z., Jeffrey, M., Lawson, F., 2000. The effect of chloride ions on the dissolution of chalcopyrite in acidic solutions. Hydrometallurgy 56 (2), 189–202.

Metz, V., Ganor, J., 2001. Stirring effect on kaolinite dissolution rate. Geochim. Cosmochim. Acta 65 (20), 3475–3490.

Mikhlin, Y.L., Romanchenko, A.S., Shagaev, A.A., 2006. Scanning probe microscopy studies of PbS surfaces oxidized in air and etched in aqueous acid solutions. Appl. Surf. Sci. 252 (16), 5645–5658.

Nicholson, R., Gillham, R., Reardon, E., 1988. Pyrite oxidation in carbonate-buffered solution I. Expermental kinetics. Geochim. Cosmochim. Acta 52 (5), 1077–1085.

Nordstrom, D., 2000. Aqueous redox chemistry and the behavior of iron in acid mine waters. In: Wilkin, R.L.R.T., Ford, R. (Eds.), Proceedings of the Workshop on Monitoring Oxidation-Reduction Processes for Ground-water Restoration, Dallas, Texas, April 25–27. Enviromental Protection Agency, pp. 43–47. EPA/600/R-02/002.

Nowak, P., Laajalehto, K., Kartio, I., 2000. A flotation related X-ray photoelectron spectroscopy study of the oxidation of galena surface. Colloids Surf., A Physicochem. Eng. Asp. 161 (3), 447–460.

Parkhurst, D., 1995. User's guide to PHREEQC: a computer program for speciation, reaction path, advective-transport, and inverse geochemical calculations. WRI USGS Geological Report, pp. 95–4227.

Pashkov, G., Mikhlina, E., Kholmogorov, A., Mikhlin, Y., 2002. Effect of potential and ferric ions on lead sulfide dissolution in nitric acid. Hydrometallurgy 63 (2), 171–179.

Pederson, L., 1982. Two-dimensional chemical-state plot for lead using XPS. J. Electron Spectrosc. Relat. Phenom. 28 (3), 203–209.

Rimstidt, J., Chermak, J., Gagen, P., 1994. Rates of reaction of galena, sphalerite, chalcopyrite and arsenopyrite with Fe(III) in acidic solutions. In: Alpers, A., Blowes, D. (Eds.), Environmental Geochemistry of Sulphide Oxidation. American Chemical Symposium Series, vol. 550. American Chemical Society, Washington D.C., pp. 2–13.

Smart, R.S.C., Skinner, W., Gerson, A., 1999. XPS of sulphide mineral surfaces: metal-deficient, polysulphides, defects and elemental sulphur. Surf. Interface Anal. 28 (1), 101–105.

Sun, Z., Forsling, W., Ronngren, L., Sjoberg, S., 1991. Surface-reactions in aqueous metal sulfide systems. i. fundamental surface-reactions of hydrous pbs and zns. Int. J. Miner. Process. 33 (1-4), 83–93.

Todd, E., Sherman, D., Purton, J., 2003. Surface oxidation of chalcopyrite ($CuFeS_2$) under ambient atmospheric and aqueous (pH 2–10) conditions: Cu, Fe L- and OK-edge X-ray spectroscopy. Geochim. Cosmochim. Acta 67 (12), 2137–2146.

Weisener, C., Smart, R.S.C., Gerson, A., 2003. Kinetics and mechanisms of the leaching of low Fe sphalerite. Geochim. Cosmochim. Acta 67 (5), 823–830.

Weisener, C., Smart, R.S.C., Gerson, A., 2004. A comparison of the kinetics and mechanism of acid leaching of sphalerite containing low and high concentrations of iron. Int. J. Miner. Process. 74 (1–4), 239–249.

Williamson, M., Rimstidt, J., 1994. The kinetics and electrochemical rate-determining step of aqueous pyrite oxidation. Geochim. Cosmochim. Acta 58 (24), 5443–5454.

Zhang, S., Li, J., Wang, Y., Hu, G., 2004. Dissolution kinetics of galena in acid NaCl solutions at 25–75 °C. Appl. Geochem. 19 (6), 835–841.

Zinng, D., Hercules, D., 1978. Electron-spectroscopy for chemical-analysis studies of lead sulfide oxidation. J. Phys. Chem. 82 (18), 1992–1995.